99.92%-Fidelity CNOT Gates in Solids by Noise Filtering

Tianyu Xie,[1,2,*] Zhiyuan Zhao,[1,2,*] Shaoyi Xu,[1,2] Xi Kong,[3] Zhiping Yang,[1,2] Mengqi Wang,[1,2] Ya Wang,[1,2,4] Fazhan Shi,[1,2,4,5,†] and Jiangfeng Du[1,2,4,‡]

[1]*CAS Key Laboratory of Microscale Magnetic Resonance and School of Physical Sciences, University of Science and Technology of China, Hefei 230026, China*

[2]*CAS Center for Excellence in Quantum Information and Quantum Physics, University of Science and Technology of China, Hefei 230026, China*

[3]*National Laboratory of Solid State Microstructures and Department of Physics, Nanjing University, Nanjing 210093, China*

[4]*Hefei National Laboratory, University of Science and Technology of China, Hefei 230088, China*

[5]*School of Biomedical Engineering and Suzhou Institute for Advanced Research, University of Science and Technology of China, Suzhou 215123, China*

(Received 30 September 2022; accepted 21 December 2022; published 19 January 2023)

Inevitable interactions with the reservoir largely degrade the performance of entangling gates, which hinders practical quantum computation from coming into existence. Here, we experimentally demonstrate a 99.920(7)%-fidelity controlled-NOT gate by suppressing the complicated noise in a solid-state spin system at room temperature. We found that the fidelity limited at 99% in previous works results from considering only static classical noise, and, thus, in this work, a complete noise model is constructed by also considering the time dependence and the quantum nature of the spin bath. All noises in the model are dynamically corrected by an exquisitely designed shaped pulse, giving the resulting error below 10^{-4}. The residual gate error is mainly originated from the longitudinal relaxation and the waveform distortion that can both be further reduced technically. Our noise-resistant method is universal and will benefit other solid-state spin systems.

DOI: 10.1103/PhysRevLett.130.030601

High-fidelity entangling gates play a crucial role in quantum information processing, in particular, fault-tolerant quantum computation [1]. However, inevitable interactions with the reservoir dramatically degrade the performance of the desired gates, especially for solid-state systems. After decades of efforts, quantum systems like superconducting circuits [2], trapped ions [3], solid-state defects [4,5], and quantum dots [6,7] have demonstrated entangling gates with fidelities above the surface-code threshold (about 99%) for fault tolerance [8,9], but practical quantum computation demands a fidelity of at least 99.9% [10]. So far, the fidelity of 99.9% has been reached for trapped ions [11–14] but still remains elusive for solid-state systems due to the noisy environment in solids.

The gate errors on logical qubits can be rendered arbitrarily small by quantum error correction provided that the errors on physical qubits are below a certain threshold [1,8–10]. Similarly, the physical errors can be further corrected dynamically among multiple primitive gates once the non-Markovian nature embraced by the noise is reasonably harnessed [15,16]. Therefore, by combining these two levels of error correction, the fidelity threshold on primitive gates could be substantially lowered, thus providing a feasible approach to practical quantum computation supported by real-world imperfect devices. However, it is experimentally hard to achieve higher-fidelity gates after error correction owing to much extra circuit complexity incurred by the correction process. Recently, universal gates on logical qubits have been demonstrated but still perform much worse than those on physical qubits [17]. The same situation appears when the method of dynamical error correction (DEC) is applied for entangling gates, because the noise characteristics for canceling the errors in between control pulses are not precisely grasped [4,18,19], and more pulses and longer gate times may result in larger errors.

Over the past decades, the high-fidelity operations enhanced by DEC are mainly single-qubit gates [4,20–22], where the special case is the identity operation spanning a long duration through dynamical decoupling [23–25]. Although there are many theoretical schemes to realize DEC-improved two-qubit gates [26–29], experimental realization remains intractable due to idealized system description and noise modeling. In this work, the reservoir noise is precisely measured and nearly 2 orders of magnitude suppressed via DEC in a solid-state spin system, namely, the nitrogen-vacancy (NV) center in diamond at room temperature. The fidelity of the CNOT gate realized here is improved from 99.52(2)% (primitive) to 99.920(7)%, both estimated by the method of randomized benchmarking [30,31].

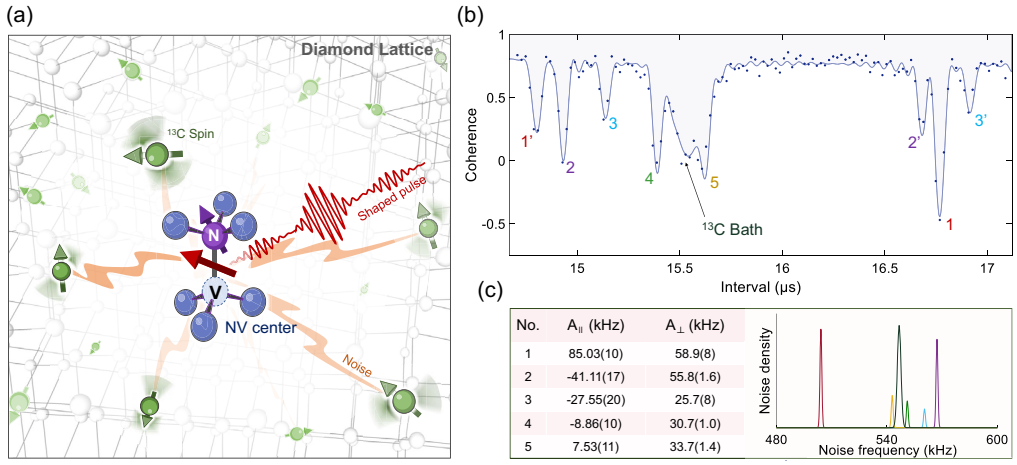

FIG. 1. Characterization of the solid-state spin system and its reservoir. (a) Schematic of a single NV center in diamond lattice. The coherence of the NV electron spin is severely disturbed by the surrounding ^{13}C nuclear spins. The proximal five ^{13}C nuclear spins are strongly coupled to the NV center and, thus, taken as quantum noise, as measured and displayed in (b) and (c). The other ^{13}C spins are effectively considered as classical noise containing static and time-varying components. The shaped pulse is employed to dynamically correct the errors caused by the noises above. (b) Detection of the ^{13}C-nuclear-spin reservoir with the NV spin coherence under a DD-32 sequence. The horizontal axis is the interval τ between two π pulses (see Supplemental Material [32]). The signatures of the proximal five ^{13}C spins (dips 1–5) emerge around the ninth resonance dip (the order $k = 9$) corresponding to the interval $\tau = (2k-1)\pi/\omega_C$, where ω_C is the ^{13}C Larmor precession frequency under a magnetic field of ≈510 G. Dip 1′ belongs to $k = 8$, while dips 2′ and 3′ belong to $k = 10$. The solid line represents the coherence curve calculated based on the coupling parameters from (c). (c) The coupling parameters of the five ^{13}C spins by fitting the results with different orders under the DD-32 sequence and the accordingly calculated noise spectrum under a magnetic field of about 510 G. $A_\parallel$ and $A_\perp$ represent the hyperfine components A_{zz} and $\sqrt{A_{zx}^2 + A_{zy}^2}$, respectively. All errors in parentheses are one standard deviation.

As illustrated in Fig. 1(a), the NV center is formed by a substitutional nitrogen atom and an adjacent vacancy in diamond lattice. The diamond used in this work is prepared with ^{13}C natural abundance (1.1%) (see Supplemental Material [32]), which brings two advantages: One is that strongly coupled ^{13}C spins are retained and available for extra quantum resources [18,36,37]; the other is avoiding costly ^{12}C isotope purification [38]. The spin coherence of the NV electron is heavily disturbed by three kinds of noise sources existing in diamond: the electron spins owned by lattice defects, ^{13}C nuclear spins, and lattice vibrations. In general, the noise from lattice defects is negligible for ultrapure diamond with high-temperature annealing. The effect of lattice vibrations is limiting the longitudinal relaxation time of the NV spin whose error is not resistable by DEC due to its Markovian behavior but can be reduced orders of magnitude at cryogenic temperatures [39]. Therefore, the noise considered to be resisted is mainly originated from the ^{13}C nuclear spins that are coupled to the NV electron spin with magnetic dipolar interactions.

Different from the previous works where the ^{13}C spin noise is simply taken as static [4,18,19], a complete noise model is constructed here by precisely measuring the ^{13}C spin environment. Generally, the ^{13}C spins in the reservoir are categorized into two groups, that is, the strongly coupled ^{13}C spins in proximity and the other weakly coupled ^{13}C spins, as shown in Fig. 1(a). Five strongly coupled ^{13}C spins are detected by monitoring the NV coherence under dynamical decoupling (DD) sequences [39,40], as shown in Fig. 1(b). The coupling parameters of the five ^{13}C spins are obtained by fitting each resonance dip (see more details in Supplemental Material [32]), with their results gathered in the table in Fig. 1(c). In the weak coupling limit, the parallel component $A_\parallel$ of the ^{13}C hyperfine interaction transitions into classical static noise, while the transverse component $A_\perp$ under the ^{13}C spin precession performs like time-varying noise. Therefore, the residual noise from the weakly coupled ^{13}C spins is treated as classical, including static and time-dependent components. The static component obeys a zero-mean Gaussian distribution with the strength measured to be $\sigma \approx 20$ kHz. The time-varying part $\eta(t)$ has two quadrature amplitudes X and Y with the strengths measured to be $\sigma_x = \sigma_y \approx 30$ kHz and is given by $\eta(t) = X\cos(\omega_C t) + Y\sin(\omega_C t)$ with ω_C denoting the ^{13}C Larmor precession frequency (see Supplemental Material [32]). The five ^{13}C spins are also classicized with the time-varying components displayed on the right in Fig. 1(c), for analyzing the noise-filtering behavior of the designed pulses in Fig. 2(a).

With the noise model above, the shaped pulse is designed to cancel the errors arising therefrom for achieving a high-fidelity CNOT gate. The CNOT gate is

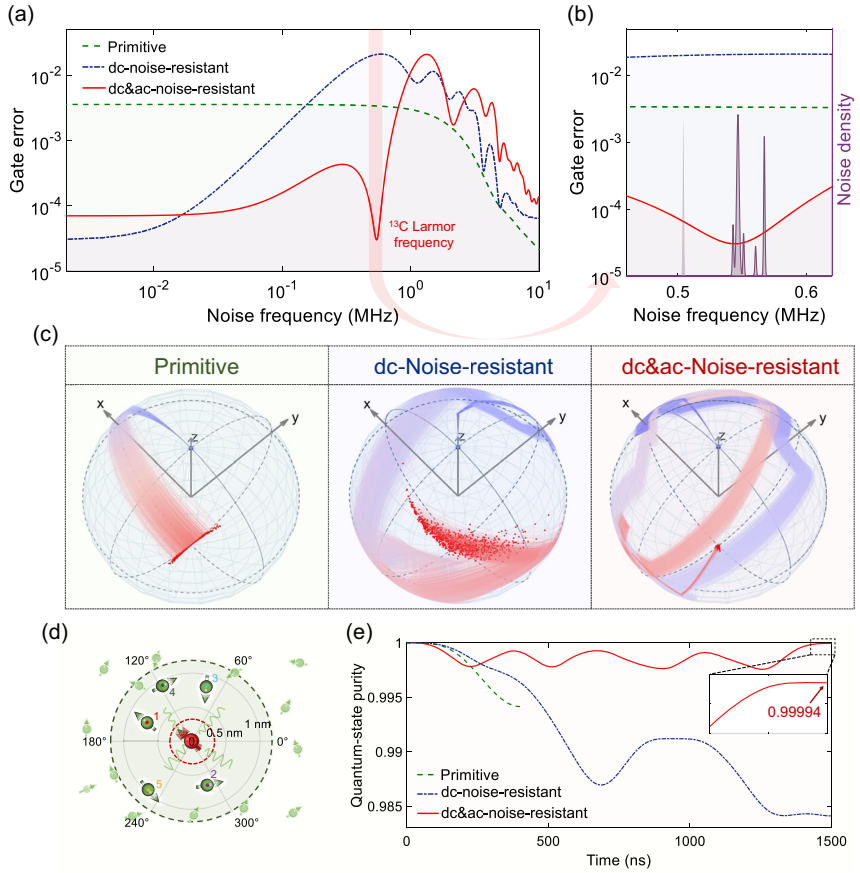

FIG. 2. Resistance to time-dependent noise and quantum noise. (a) The CNOT gate error induced by time-dependent noise for three kinds of control pulses. The primitive gate is realized by a rectangular pulse (green), while the other two are constructed by shaped pulses to dynamically correct the noise-induced errors, of which the one is optimized to resist only static noise (blue) and the other is resistant to both static and time-varying noises (red). In the calculation, two components of the time-dependent noise obey Gaussian distributions with the strengths $\sigma_x = \sigma_y = 70$ kHz. (b) The enlarged display near the ^{13}C Larmor frequency in (a), together with the ^{13}C noise spectrum [Fig. 1(c)]. (c) The state evolution under the NOT operation of the CNOT gate with 1000 samples of the time-varying noise at the ^{13}C Larmor frequency. (d) Localization of the proximal five ^{13}C spins that function as quantum noise in (e). (e) Resistance to quantum noise exhibited by the quantum-state purity under the NOT operation of the CNOT gate. The five ^{13}C spins are taken as quantum objects, and their couplings to the NV center are included in the whole Hamiltonian. See the behaviors under the identity operation of the CNOT gate in Supplemental Material [32].

the nuclear-state-controlled electron NOT ($C_n NOT_e$) gate performed upon the hybrid system constituted by the NV electron spin and the ^{14}N nuclear spin. Considering the complexity of the problem, the numerical method is adopted to optimize the shaped pulse for filtering the noise with higher orders. It is worth noting that it is unnecessary to take the nearby ^{13}C spins as quantum objects in the numerical optimization, which dramatically reduces the required computation overhead and makes the optimized shaped pulse applicable for the other NVs without the need for *a priori* knowledge of the ^{13}C spin distribution (see Supplemental Material [32]).

In order to estimate the performance of the optimized pulse, the ability to resist different time-varying noises is first investigated [41,42]. The noise-filtering method, just as used in DD [24,43], is employed here for analyzing the gate fidelity by calculating the overlap integral between the filter function $F(\omega)$ and the noise spectrum $S(\omega)$. Nevertheless, due to the control-noise noncommutativity, the expression of the gate fidelity must be expanded in series [44,45]:

$$\mathcal{F}_g = 1 - \frac{1}{2\pi}\int_{-\infty}^{+\infty}\frac{d\omega}{\omega^2}S(\omega)F_1(\omega) - \frac{1}{(2\pi)^2}\int_{-\infty}^{+\infty}\frac{d\omega}{\omega^2}S(\omega)\int_{-\infty}^{+\infty}\frac{d\omega'}{\omega'^2}S(\omega')F_2(\omega,\omega') - \cdots, \tag{1}$$

where $F_1(\omega)$ and $F_2(\omega,\omega')$ are the filter functions of the first two orders. Since the noise-filtering behavior of the optimized pulse cannot be sufficiently depicted by the

leading-order term, we directly calculated the gate errors under different time-varying noises, which can serve as an all-order filter function in some sense. The results obtained for the optimized pulse with a duration of 1.5 μs are plotted in Fig. 2(a), together with those of the primitive pulse (401 ns) and another shaped pulse with only static-noise resistance (1.5 μs) for comparison. The latter performs badly near the ^{13}C Larmor frequency ω_C and even worse than the primitive pulse due to a longer duration, which justifies constructing the complete noise model instead of a simplified static one [4,18,19]. The time-varying-noise resistance near ω_C optimized for the shaped pulse also works for the proximal five ^{13}C spins with all errors near the minimum below 10^{-4}, as shown in Fig. 2(b). The performances of the pulses above manifest even more obviously by monitoring the state evolutions under 1000 noise samples at ω_C, graphically represented as the trajectories of the Bloch vector in Fig. 2(c). The trajectories for the time-varying-noise-resistant pulse finally converge into a small region, in comparison to the largely dispersed regions exhibited by the other two pulses. As a matter of fact, the effect of the strongly coupled ^{13}C spins can be precisely analyzed by absorbing them to constitute a seven-qubit quantum register, with their locations given in Fig. 2(d). Under this scenario, the quantum-state purity is utilized to evaluate the ability to resist the quantum noise from other qubits, as displayed in Fig. 2(e). The final purity is recovered above 0.9999 for the shaped pulse with time-varying noise optimized, which signifies that destructive entanglements with the ^{13}C spins are canceled out among the subpulses of the shaped pulse.

In the following, the high fidelity manifested by the shaped pulse optimized above is experimentally characterized by the Clifford-based randomized benchmarking (RB) [30,31]. However, it is inconvenient to directly apply two-qubit RB for the hybrid system here, due to the control difference between the electron spin and the nuclear spin. Alternatively, considering the negligible error from nuclear-spin decoherence [Fig. 4(d)], the two-qubit RB for the $C_n\mathrm{NOT}_e$ gate can be simplified into estimating the fidelities of the identity operation and the NOT operation in two nuclear subspaces, which is called subspace randomized benchmarking [46] (see Supplemental Material [32]). Before benchmarking the operations above by interleaved RB (IRB) [31], single-qubit RB needs to be implemented first to serve as a reference. The shaped pulse shown in Fig. 3(b) is designed for performing the $\pi/2$ gate in both subspaces defined as Fig. 3(a), from which single-qubit Cliffords are established. The average fidelities per Clifford are measured to be 99.936(4)% for the state $m_I = 0$ and 99.979(3)% for the state $m_I = +1$ by fitting the RB results in Fig. 3(c). Since every Clifford has about 2.2 $\pi/2$ gates on average, the fidelity of the $\pi/2$ gate turns out to be 99.980(1)%. As described in Fig. 2, the shaped pulse with the profile [Fig. 4(a)] is optimized to resist the complete noise model, including static and time-varying, classical,

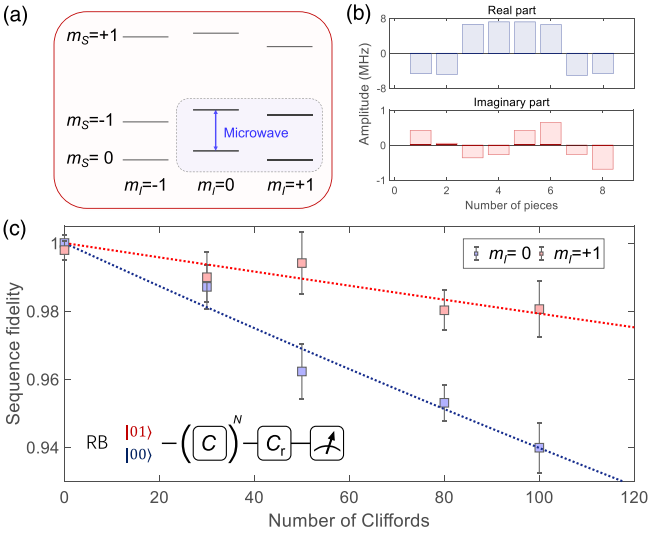

FIG. 3. Single-qubit gates and randomized benchmarking. (a) Level diagram of the NV-^{14}N coupled system. The four levels inside the shaded box are utilized as two qubits, and the microwave is resonantly applied in the spin state $m_I = 0$. (b) The optimized shaped pulse that simultaneously performs the $\pi/2$ gate in both $m_I = 0$ and $m_I = +1$ subspaces. The shaped pulse exhibits a piecewise-constant amplitude (Rabi frequency) profile with eight pieces of 30-ns subpulses in both real and imaginary parts. See more details in Supplemental Material [32]. (c) The single-qubit RB results for two nuclear spin states. The Clifford gates are comprised of the $\pi/2$ gate in (b). By fitting the results, the average fidelities per Clifford are given by 99.936 (4)% for the state $m_I = 0$ and 99.979(3)% for the state $m_I = +1$. Inset: the implemented RB sequences.

and quantum noises. The noise-resistant ability is acquired by experiencing the complicated evolutions displayed in Fig. 4(b), corresponding to the identity operation and the NOT operation in both subspaces, respectively. By applying the IRB sequences, the fidelity of the CNOT gate realized by the shaped pulse is found to be 99.920(7)% in Fig. 4(c) after subtracting the single-qubit reference. Compared with the primitive gate with a fidelity of 99.52(2)%, the shaped pulse with only static-noise resistance has a lower fidelity of 98.27(6)% for the fact that the noise model is inaccurate and a longer gate time leads to a larger error, as stated regarding DEC.

The residual error 0.80(7)‰ is accountable by scrutinizing the errors from varieties of experimental imperfections that are collected in Fig. 4(d) (see a detailed analysis in Supplemental Material [32]). After suppressing the error from the spin reservoir by 2 orders of magnitude, the errors from the longitudinal relaxation of the NV spin and the waveform distortion of the shaped pulse dominate. The error from the longitudinal relaxation for our room-temperature setup is estimated to be 0.32‰ by measuring three-level relaxation behaviors, which can be removed by running at cryogenic temperatures [39]. The error from the waveform distortion is 0.21‰ by performing the state

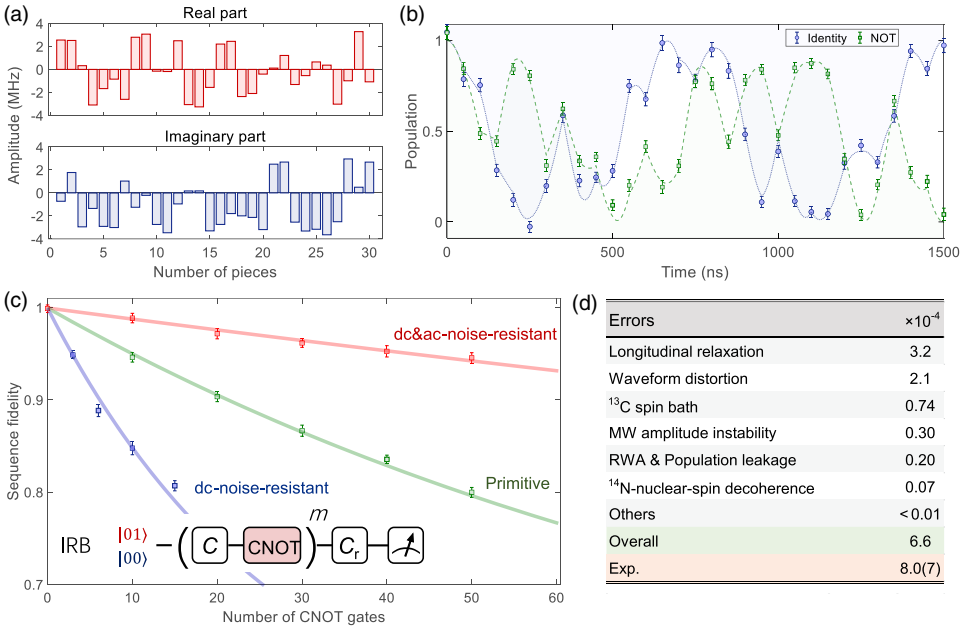

Errors	$\times 10^{-4}$
Longitudinal relaxation	3.2
Waveform distortion	2.1
^{13}C spin bath	0.74
MW amplitude instability	0.30
RWA & Population leakage	0.20
^{14}N-nuclear-spin decoherence	0.07
Others	< 0.01
Overall	6.6
Exp.	8.0(7)

FIG. 4. CNOT gates and gate error analysis. (a) The optimized shaped pulse for realizing a high-fidelity CNOT gate. As shown in Fig. 2, the shaped pulse is resistant to static noise, time-varying noise, and quantum noise. It has 30 pieces of 50-ns subpulses in both real and imaginary parts, and more details can be found in Supplemental Material [32]. (b) The measured evolutions under the NOT and identity operations of the CNOT gate by applying the shaped pulse in (a). The solid lines are the theoretical simulations. (c) The fidelity measurement of the CNOT gates realized by the pulses in Fig. 2 by the modified IRB. Inset: the implemented modified IRB sequences. (d) Error budget for the residual gate infidelity.

tomography after the IRB sequences and can be further mitigated by carefully refining the waveform details or by quantum optimal control [47,48]. The remanent error from the ^{13}C spin bath is calculated to be 0.074‰ based on the noise model above, including the five ^{13}C spins, the static noise (20 kHz), and the time-varying noise (30 kHz). Other errors are insignificant: The amplitude instability of the applied microwave produces an error of 0.030‰; the effects from the rotation wave approximation and the population leakage into the third level are calculated together to give an error of 0.020‰; the ^{14}N-nuclear-spin decoherence from the applied pulse not from the ^{13}C spin bath gives an error of 7×10^{-6}; and the errors from other sources are all below 10^{-6}.

In conclusion, we demonstrate a 99.920(7)%-fidelity CNOT gate in a solid-state spin system by employing DEC. The spin reservoir is precisely measured for establishing a complete and real noise model, consisting of static noise, time-varying noise, and quantum noise. The shaped pulse is exquisitely designed to dynamically correct the errors from all kinds of noises. The method above is extensively applicable for solid-state spin systems, such as phosphorus dopants [5,49] and quantum dots [6,7] in silicon, defects in diamond and silicon carbide [50,51], rare-earth-doped crystals [52,53], and so forth. The analysis of the residual gate error indicates that all errors above 10^{-4} can be removed technically, providing the possibility to improve the fidelity up to 99.99%. The high-fidelity CNOT gate realized here is of significant importance for practical quantum computation. Furthermore, considering being performed on a hybrid spin system, it is also crucial for exchanging quantum information between electron and nuclear spins on the interface of quantum memory [49,54].

We thank Jianpei Geng (University of Stuttgart, Germany) for helpful discussions. This work was supported by the National Key R&D Program of China (Grants No. 2018YFA0306600 and No. 2016YFA0502400), the National Natural Science Foundation of China (Grants No. 81788101, No. 91636217, No. T2125011, and No. 12274396), Innovation Program for Quantum Science and Technology (Grants No. 2021ZD0302200 and No. 2021ZD0303204), the CAS (Grants No. XDC07000000, No. GJJSTD20200001, No. QYZDY-SSW-SLH004, and No. Y201984), the Anhui Initiative in Quantum Information Technologies (Grant No. AHY050000), the Fundamental Research Funds for the Central Universities, the China Postdoctoral Science Foundation (Grants No. 2021M703110 and No. 2022T150631), and the Hefei Comprehensive National Science Center.

*These authors contributed equally to this work.
†fzshi@ustc.edu.cn
‡djf@ustc.edu.cn

[1] M. A. Nielsen and I. L. Chuang, *Quantum Computation and Quantum Information* (Cambridge University Press, Cambridge, England, 2000).

[2] R. Barends, J. Kelly, A. Megrant, A. Veitia, D. Sank, E. Jeffrey, T. C. White, J. Mutus, A. G. Fowler, B. Campbell *et al.*, Superconducting quantum circuits at the surface code threshold for fault tolerance, Nature (London) **508**, 500 (2014).

[3] J. Benhelm, G. Kirchmair, C. F. Roos, and R. Blatt, Towards fault-tolerant quantum computing with trapped ions, Nat. Phys. **4**, 463 (2008).

[4] X. Rong, J. Geng, F. Shi, Y. Liu, K. Xu, W. Ma, F. Kong, Z. Jiang, Y. Wu, and J. Du, Experimental fault-tolerant universal quantum gates with solid-state spins under ambient conditions, Nat. Commun. **6**, 8748 (2015).

[5] M. T. Mądzik, S. Asaad, A. Youssry, B. Joecker, K. M. Rudinger, E. Nielsen, K. C. Young, T. J. Proctor, A. D. Baczewski, A. Laucht *et al.*, Precision tomography of a three-qubit donor quantum processor in silicon, Nature (London) **601**, 348 (2022).

[6] A. Noiri, K. Takeda, T. Nakajima, T. Kobayashi, A. Sammak, G. Scappucci, and S. Tarucha, Fast universal quantum gate above the fault-tolerance threshold in silicon, Nature (London) **601**, 338 (2022).

[7] X. Xue, M. Russ, N. Samkharadze, B. Undseth, A. Sammak, G. Scappucci, and L. M. Vandersypen, Quantum logic with spin qubits crossing the surface code threshold, Nature (London) **601**, 343 (2022).

[8] R. Raussendorf and J. Harrington, Fault-Tolerant Quantum Computation with High Threshold in Two Dimensions, Phys. Rev. Lett. **98**, 190504 (2007).

[9] D. S. Wang, A. G. Fowler, and L. C. L. Hollenberg, Surface code quantum computing with error rates over 1%, Phys. Rev. A **83**, 020302(R) (2011).

[10] A. G. Fowler, M. Mariantoni, J. M. Martinis, and A. N. Cleland, Surface codes: Towards practical large-scale quantum computation, Phys. Rev. A **86**, 032324 (2012).

[11] C. J. Ballance, T. P. Harty, N. M. Linke, M. A. Sepiol, and D. M. Lucas, High-Fidelity Quantum Logic Gates using Trapped-Ion Hyperfine Qubits, Phys. Rev. Lett. **117**, 060504 (2016).

[12] J. P. Gaebler, T. R. Tan, Y. Lin, Y. Wan, R. Bowler, A. C. Keith, S. Glancy, K. Coakley, E. Knill, D. Leibfried *et al.*, High-Fidelity Universal Gate Set for $^{9}Be^{+}$ Ion Qubits, Phys. Rev. Lett. **117**, 060505 (2016).

[13] C. R. Clark, H. N. Tinkey, B. C. Sawyer, A. M. Meier, K. A. Burkhardt, C. M. Seck, C. M. Shappert, N. D. Guise, C. E. Volin, S. D. Fallek *et al.*, High-Fidelity Bell-State Preparation with $^{40}Ca^{+}$ Optical Qubits, Phys. Rev. Lett. **127**, 130505 (2021).

[14] R. Srinivas, S. C. Burd, H. M. Knaack, R. T. Sutherland, A. Kwiatkowski, S. Glancy, E. Knill, D. J. Wineland, D. Leibfried, A. C. Wilson *et al.*, High-fidelity laser-free universal control of trapped ion qubits, Nature (London) **597**, 209 (2021).

[15] K. Khodjasteh and L. Viola, Dynamically Error-Corrected Gates for Universal Quantum Computation, Phys. Rev. Lett. **102**, 080501 (2009).

[16] K. Khodjasteh, D. A. Lidar, and L. Viola, Arbitrarily Accurate Dynamical Control in Open Quantum Systems, Phys. Rev. Lett. **104**, 090501 (2010).

[17] L. Postler, S. Heußen, I. Pogorelov, M. Rispler, T. Feldker, M. Meth, C. D. Marciniak, R. Stricker, M. Ringbauer, R. Blatt *et al.*, Demonstration of fault-tolerant universal quantum gate operations, Nature (London) **605**, 675 (2022).

[18] G. Waldherr, Y. Wang, S. Zaiser, M. Jamali, T. Schulte-Herbrüggen, H. Abe, T. Ohshima, J. Isoya, J. Du, P. Neumann *et al.*, Quantum error correction in a solid-state hybrid spin register, Nature (London) **506**, 204 (2014).

[19] F. Dolde, V. Bergholm, Y. Wang, I. Jakobi, B. Naydenov, S. Pezzagna, J. Meijer, F. Jelezko, P. Neumann, T. Schulte-Herbrüggen *et al.*, High-fidelity spin entanglement using optimal control, Nat. Commun. **5**, 3371 (2014).

[20] A. Soare, H. Ball, D. Hayes, J. Sastrawan, M. C. Jarratt, J. J. McLoughlin, X. Zhen, T. J. Green, and M. J. Biercuk, Experimental noise filtering by quantum control, Nat. Phys. **10**, 825 (2014).

[21] P. Cerfontaine, T. Botzem, J. Ritzmann, S. S. Humpohl, A. Ludwig, D. Schuh, D. Bougeard, A. D. Wieck, and H. Bluhm, Closed-loop control of a GaAs-based singlet-triplet spin qubit with 99.5% gate fidelity and low leakage, Nat. Commun. **11**, 4144 (2020).

[22] M. Werninghaus, D. J. Egger, F. Roy, S. Machnes, F. K. Wilhelm, and S. Filipp, Leakage reduction in fast superconducting qubit gates via optimal control, npj Quantum Inf. **7**, 14 (2021).

[23] J. Du, X. Rong, N. Zhao, Y. Wang, J. Yang, and R. Liu, Preserving electron spin coherence in solids by optimal dynamical decoupling, Nature (London) **461**, 1265 (2009).

[24] M. J. Biercuk, H. Uys, A. P. VanDevender, N. Shiga, W. M. Itano, and J. J. Bollinger, Optimized dynamical decoupling in a model quantum memory, Nature (London) **458**, 996 (2009).

[25] G. de Lange, Z.-H. Wang, D. Riste, V. Dobrovitski, and R. Hanson, Universal dynamical decoupling of a single solid-state spin from a spin bath, Science **330**, 60 (2010).

[26] S. Montangero, T. Calarco, and R. Fazio, Robust Optimal Quantum Gates for Josephson Charge Qubits, Phys. Rev. Lett. **99**, 170501 (2007).

[27] J. L. Allen, R. Kosut, J. Joo, P. Leek, and E. Ginossar, Optimal control of two qubits via a single cavity drive in circuit quantum electrodynamics, Phys. Rev. A **95**, 042325 (2017).

[28] Y. Chou, S.-Y. Huang, and H.-S. Goan, Optimal control of fast and high-fidelity quantum gates with electron and nuclear spins of a nitrogen-vacancy center in diamond, Phys. Rev. A **91**, 052315 (2015).

[29] C.-H. Huang, C.-H. Yang, C.-C. Chen, A. S. Dzurak, and H.-S. Goan, High-fidelity and robust two-qubit gates for quantum-dot spin qubits in silicon, Phys. Rev. A **99**, 042310 (2019).

[30] E. Magesan, J. M. Gambetta, and J. Emerson, Scalable and Robust Randomized Benchmarking of Quantum Processes, Phys. Rev. Lett. **106**, 180504 (2011).

[31] E. Magesan, J. M. Gambetta, B. R. Johnson, C. A. Ryan, J. M. Chow, S. T. Merkel, M. P. da Silva, G. A. Keefe, M. B. Rothwell, T. A. Ohki, M. B. Ketchen, and M. Steffen, Efficient Measurement of Quantum Gate Error by Interleaved Randomized Benchmarking, Phys. Rev. Lett. **109**, 080505 (2012).

[32] See Supplemental Material at http://link.aps.org/supplemental/10.1103/PhysRevLett.130.030601 for additional details on experimental methods, construction of the noise model, optimization of shaped pulses, subspace randomized benchmarking, and gate error analysis, which includes Refs. [33–35].

[33] T. Xie, Z. Zhao, M. Guo, M. Wang, F. Shi, and J. Du, Identity Test of Single NV^- Centers in Diamond at Hz-Precision Level, Phys. Rev. Lett. **127**, 053601 (2021).

[34] N. Khaneja, T. Reiss, C. Kehlet, T. Schulte-Herbrüggen, and S. J. Glaser, Optimal control of coupled spin dynamics: Design of NMR pulse sequences by gradient ascent algorithms, J. Magn. Reson. **172**, 296 (2005).

[35] L. H. Pedersen, N. M. Møller, and K. Mølmer, Fidelity of quantum operations, Phys. Lett. A **367**, 47 (2007).

[36] C. E. Bradley, J. Randall, M. H. Abobeih, R. C. Berrevoets, M. J. Degen, M. A. Bakker, M. Markham, D. J. Twitchen, and T. H. Taminiau, A Ten-Qubit Solid-State Spin Register with Quantum Memory Up to One Minute, Phys. Rev. X **9**, 031045 (2019).

[37] T. Xie, Z. Zhao, X. Kong, W. Ma, M. Wang, X. Ye, P. Yu, Z. Yang, S. Xu, P. Wang *et al.*, Beating the standard quantum limit under ambient conditions with solid-state spins, Sci. Adv. **7**, eabg9204 (2021).

[38] G. Balasubramanian, P. Neumann, D. Twitchen, M. Markham, R. Kolesov, N. Mizuochi, J. Isoya, J. Achard, J. Beck, J. Tissler *et al.*, Ultralong spin coherence time in isotopically engineered diamond, Nat. Mater. **8**, 383 (2009).

[39] M. H. Abobeih, J. Cramer, M. A. Bakker, N. Kalb, M. Markham, D. J. Twitchen, and T. H. Taminiau, One-second coherence for a single electron spin coupled to a multi-qubit nuclear-spin environment, Nat. Commun. **9**, 2552 (2018).

[40] T. H. Taminiau, J. J. T. Wagenaar, T. van der Sar, F. Jelezko, V. V. Dobrovitski, and R. Hanson, Detection and Control of Individual Nuclear Spins using a Weakly Coupled Electron Spin, Phys. Rev. Lett. **109**, 137602 (2012).

[41] C. Kabytayev, T. J. Green, K. Khodjasteh, M. J. Biercuk, L. Viola, and K. R. Brown, Robustness of composite pulses to time-dependent control noise, Phys. Rev. A **90**, 012316 (2014).

[42] C.-H. Huang and H.-S. Goan, Robust quantum gates for stochastic time-varying noise, Phys. Rev. A **95**, 062325 (2017).

[43] W. Ma, F. Shi, K. Xu, P. Wang, X. Xu, X. Rong, C. Ju, C.-K. Duan, N. Zhao, and J. Du, Resolving remote nuclear spins in a noisy bath by dynamical decoupling design, Phys. Rev. A **92**, 033418 (2015).

[44] T. Green, H. Uys, and M. J. Biercuk, High-Order Noise Filtering in Nontrivial Quantum Logic Gates, Phys. Rev. Lett. **109**, 020501 (2012).

[45] G. A. Paz-Silva and L. Viola, General Transfer-Function Approach to Noise Filtering in Open-Loop Quantum Control, Phys. Rev. Lett. **113**, 250501 (2014).

[46] C. H. Baldwin, B. J. Bjork, J. P. Gaebler, D. Hayes, and D. Stack, Subspace benchmarking high-fidelity entangling operations with trapped ions, Phys. Rev. Res. **2**, 013317 (2020).

[47] J. Li, X. Yang, X. Peng, and C.-P. Sun, Hybrid Quantum-Classical Approach to Quantum Optimal Control, Phys. Rev. Lett. **118**, 150503 (2017).

[48] D. Wierichs, J. Izaac, C. Wang, and C. Y.-Y. Lin, General parameter-shift rules for quantum gradients, Quantum **6**, 677 (2022).

[49] J. J. L. Morton, A. M. Tyryshkin, R. M. Brown, S. Shankar, B. W. Lovett, A. Ardavan, T. Schenkel, E. E. Haller, J. W. Ager, and S. A. Lyon, Solid-state quantum memory using the ^{31}P nuclear spin, Nature (London) **455**, 1085 (2008).

[50] M. Widmann, S.-Y. Lee, T. Rendler, N. T. Son, H. Fedder, S. Paik, L.-P. Yang, N. Zhao, S. Yang, I. Booker *et al.*, Coherent control of single spins in silicon carbide at room temperature, Nat. Mater. **14**, 164 (2015).

[51] G. Wolfowicz, F. J. Heremans, C. P. Anderson, S. Kanai, H. Seo, A. Gali, G. Galli, and D. D. Awschalom, Quantum guidelines for solid-state spin defects, Nat. Rev. Mater. **6**, 906 (2021).

[52] P. Siyushev, K. Xia, R. Reuter, M. Jamali, N. Zhao, N. Yang, C. Duan, N. Kukharchyk, A. Wieck, R. Kolesov *et al.*, Coherent properties of single rare-earth spin qubits, Nat. Commun. **5**, 3895 (2014).

[53] A. Ruskuc, C.-J. Wu, J. Rochman, J. Choi, and A. Faraon, Nuclear spin-wave quantum register for a solid-state qubit, Nature (London) **602**, 408 (2022).

[54] P. C. Maurer, G. Kucsko, C. Latta, L. Jiang, N. Y. Yao, S. D. Bennett, F. Pastawski, D. Hunger, N. Chisholm, M. Markham *et al.*, Room-temperature quantum bit memory exceeding one second, Science **336**, 1283 (2012).